Laser absorption and hot electron temperature scalings in laser–plasma interactions

5 authors, including:

Wei-Min Wang
Department of Physics
159 PUBLICATIONS   **2,598** CITATIONS

Yu Tong Li
Chinese Academy of Sciences
303 PUBLICATIONS   **4,804** CITATIONS

Jie Zhang
1,228 PUBLICATIONS   **22,613** CITATIONS

Some of the authors of this publication are also working on these related projects:

Project   Laser plasma interaction View project

Project   High quality ionization injections in laser wakefield accelerators View project

Laser absorption and hot electron temperature scalings in laser–plasma interactions

Laser absorption and hot electron temperature scalings in laser–plasma interactions

Yun-Qian Cui[1], Wei-Min Wang[1], Zheng-Ming Sheng[1,2], Yu-Tong Li[1] and Jie Zhang[1,2]

[1] Beijing National Laboratory of Condensed Matter Physics, Institute of Physics, CAS, Beijing 100190, People's Republic of China
[2] Key Laboratory for Laser Plasmas (MoE) and Department of Physics, Shanghai Jiao Tong University, Shanghai 200240, People's Republic of China

E-mail: zmsheng@sjtu.edu.cn

Abstract
Laser absorption in the interaction between ultra-intense femtosecond laser and solid density plasma is studied integratedly for the intensity range $I\lambda^2 \simeq 10^{14}$–$10^{20}$ W cm^{-2} μm^2 by particle-in-cell simulations with collision modulus included. The collisional effect is found to be significant when the incident laser intensity is less than 10^{16} W cm^{-2} μm^2, which tends to enhance the resonance absorption and reduce the vacuum heating under different plasma parameters. At higher intensities, various collisionless absorption mechanisms dominate with a large number of hot electrons produced. The scaling of hot electron temperatures is found to depend upon the dominant absorption mechanisms. At moderate intensity around 10^{17} W cm^{-2}, the scaling law is $T_{\mathrm{hot}} \propto (I\lambda^2)^{1/3}$ when the incident angle matches the optimized angle of resonance absorption; otherwise, $T_{\mathrm{hot}} \propto (I\lambda^2)^{\alpha}$ with $\alpha > 1/3$, which changes with laser incident angles and preplasma scale lengths; in the case of vacuum heating, usually $\alpha > 1$. At laser intensity above 10^{18} W cm^{-2} μm^2 when the absorption mechanism is dominated by ponderomotive acceleration, the scaling becomes $T_{\mathrm{hot}} \propto (I\lambda^2)^{1/2}$. The angular distributions of hot electrons are also shown to be dependent upon the absorption mechanisms.

(Some figures may appear in colour only in the online journal)

1. Introduction

The fraction of laser absorption during the interaction between ultrashort ultra-intense laser and dense plasma is a key problem of fast ignition scheme [1, 2], ion acceleration [3–6] and high energy density matter production [7–9]. A series of mechanisms is proposed to explain the absorptions observed under different laser and plasma conditions. For example, collisional absorption, resonance absorption, vacuum heating and other collisionless absorption dominate the absorption separately in different intensity ranges. When collisional effect is vigorous, a mechanism named collisional absorption or inverse bremsstrahlung contributes a lot to the total absorption [10, 11]. However, since the collision frequency reduces as the effective temperature increases, it becomes negligible when laser intensity is sufficiently high. When the laser is

p-polarized and incident obliquely, depending on the ultimate parameter $v_{\mathrm{osc}}/(\omega L)$, it is possible for two other absorption mechanisms to occur separately [12]. Here L denotes the preplasma density scale length, ω denotes the laser frequency, and $v_{\mathrm{osc}} = eE/(m_{\mathrm{e}}\omega)$ is the quiver velocity of the electron, in which E and ω represent laser electric field and laser frequency, respectively. When L is large, a component of laser electric vector oscillates electrons along the direction of the density gradient, an electron electrostatic wave (ESW) can be excited and part of the laser energy is transferred to the ESW. This is called resonance absorption [13–15], which can be very efficient when the laser incident angle matches the plasma density gradient. It can be significant either at low or high laser intensity. Along with the increase in the incident laser intensity, relativistic effect can change the resonance absorption considerably [16–18]. On the other

hand, if the preplasma density profile is very steep or $L \ll \lambda$ with λ the laser wavelength, the electrons can be pulled into vacuum and sent back to the plasma with the quiver velocity $v_{osc} \sim c$, this can also lead to a large absorption called vacuum heating [14, 19, 20]. After the laser intensity reaches as high as 10^{18} W cm^{-2} μm^2, the ponderomotive force is strong enough to push electrons forward in the incident direction, this process transfers laser energy to the electrons significantly, which is called $\boldsymbol{j} \times \boldsymbol{B}$ heating or ponderomotive force heating [15, 21, 22]. One notes that in the relativistic high-intensity regime, it is found recently that vacuum heating and $\boldsymbol{j} \times \boldsymbol{B}$ heating can be described in a unified way in the case with a steep density profile [23].

So far, some experiments have been conducted to measure the absorption rates in a certain range of laser intensity [24–27]. However, a comprehensive investigation of absorption rate in a large laser-intensity range is still not available either experimentally or numerically. The purpose of this paper is to clarify the transitions and conditions of different absorption mechanisms found in a wide range of intensities from $I\lambda^2 = 1.37 \times 10^{14}$ W cm^{-2} μm^2 to 1.37×10^{20} W cm^{-2} μm^2, based upon a series of 2D3V particle-in-cell (PIC) simulations. This numerical survey can be useful to explain the existing experimental results on laser absorption and hot electron production for a wide intensity range.

The paper is arranged as follows. In section 2, intensity-dependent absorption rate is presented with collisional effect included in our simulations. At a high laser intensity above 10^{17} W cm^{-2}, the laser absorption directly leads to hot electron production. In section 3, the scalings of hot electron production due to different mechanisms are discussed. Previous experiments find power scaling of hot electron temperature, i.e. $T_{hot} \propto (I\lambda^2)^\alpha$. However, various values of α were reported from different experiments [25, 28–30]. Our simulation results indicate that the temperature scaling is strongly dependent on the absorption mechanisms, which also lead to different hot electron angular distributions. Finally conclusions are drawn in section 4.

2. Intensity-dependent absorption rate

The simulations are executed by our self-encoded 2D3V PIC code KLAPS [31, 32]. We include binary Coulomb collision between e–e, e–i and i–i in our code using an algorithm based on [33]. The collision modulus is examined according to Landau's analytical theory of balancing between different temperature components [34] and collisional absorption [13].

In our simulations, the p-polarized laser at 800 nm is incident from the left boundary of the simulation box at different angles. The amplitude profile of the vector potential is given by $a = a_0 \exp(-r^2/w_0^2) \sin^2(\pi t/\tau_0)$, which is normalized by $m_e \omega c/e$. The peak amplitude a_0 is related to the laser intensity by $I\lambda^2 = a_0^2 \times 1.37 \times 10^{18}$ W cm^{-2} μm^2. The laser pulse duration and focus spot waist radius are taken as $\tau_0 = 20\tau = 53.3$ fs and $w_0 = 5\lambda = 4$ μm. The target is uniform in the y-direction, the density profiles in the x-direction of different preplasma cases are shown in figure 1, in which $n_{max} = 3\gamma_{osc} n_c$. Here $n_c = m_e \omega^2/(4\pi e^2)$ is the
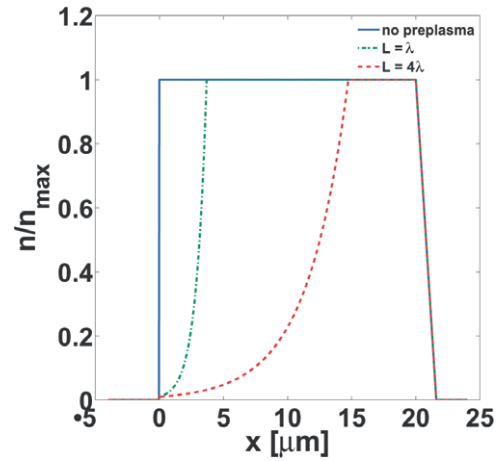

Figure 1. The density profile along the x-axis. If preplasma exists, the density increases exponentially from $n_{max}/100$ to n_{max} with scale length L.

non-relativistic critical density and $\gamma_{osc} = \sqrt{1 + a_0^2}$ is the Lorentz factor related to the quiver oscillation of electrons in the laser electric field. It is worth mentioning that this maximal density is not enough to resolve the absorption mechanism based on skin effects such as inverse bremsstrahlung or anomalous skin effect [35], which could also contribute a considerable fraction at real solid density with a step density profile. The ion–electron mass ratio is set to 1836 and the initial temperature of both electrons and ions is set as 100 eV. The size of the simulation box is $87\lambda \times 122\lambda$ resolved by 1740×2440 grids with 25 particles per cell. Particles are advanced with a time step of 0.01τ. Absorption boundary condition is implemented in both x- and y-directions. The absorption rates are calculated from the incident, reflected, transmitted and scattered electromagnetic wave energy by $1 - (E_{ref} + E_{tra} + E_{sca})/E_{inc}$. A virtual frame is placed around the target to monitor the emergent energy flux. $E_{ref} + E_{tra} + E_{sca}$ can be obtained easily by integrating the energy flux over the frame boundary and time.

Figure 2 shows the absorption rate as a function of the laser intensity $I\lambda^2$ at different incident angles θ and preplasma density scale lengths L with and without collision. The results from our simulation are generally in good agreement with the experimental results given in [26] under similar conditions regardless of ion species. Generally, the absorption rate depends upon the preplasma density scale length L, the laser incident angle θ, the laser intensity $I\lambda^2$, as well as plasma collision effect.

Comparing the solid and dashed curves in figure 2, one can see significant absorption is caused by the collision effect at low intensities $I\lambda^2 \leqslant 10^{16}$ W cm^{-2} μm^2. The absorption decreases as incident laser becomes intense. This is because the electron collision frequency is in inverse ratio to the effective temperature $T_e + E_{osc}$, where E_{osc} is the quiver energy of electrons. The collision effect is negligible when the laser intensity $I\lambda^2$ reaches 10^{17} W cm^{-2} μm^2. It can also be seen from figure 2 that collisional absorption increases with the growth of density scale length and decreases with the increase
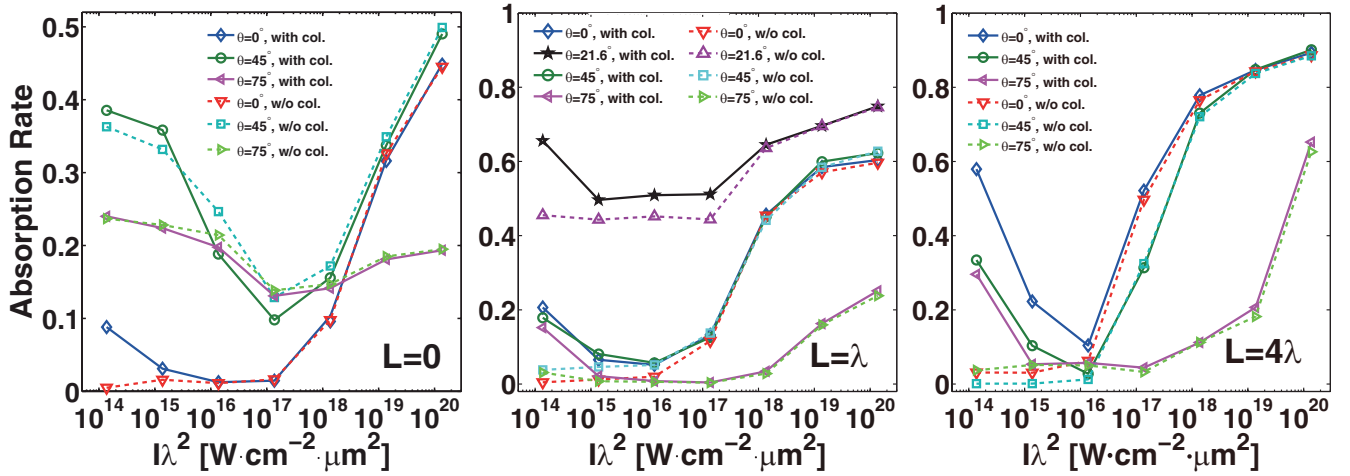
Figure 2. Absorption rate versus laser intensity $I\lambda^2$ under normal, 45° and 75° incidence with different preplasma conditions. For $L = \lambda$ case, 21.6° incidence is also calculated because it is calculated to be the optimized incident angle for resonance absorption. Abbreviation 'col.' and 'w/o' represent 'collision' and 'without', respectively.

in incident angle, which is in agreement with Kruer's analytical prediction [13].

$$f_A = 1 - \exp\left(-\frac{8\nu_{ei}^* L}{3c} \cos^3\theta\right). \quad (1)$$

This is against the statement in [21], which says inverse bremsstrahlung decreases for long scale lengths. It demands more theoretical and experimental work to clarify this conflict.

In addition to the collisional absorption, in the case of oblique incidence of the p-polarized laser pulse, some other absorption mechanism can also be very obvious. Figure 2(a) shows the condition of no preplasma, i.e. $L = 0$, one can find that the absorption rates under 45° incidence are larger than normal incidence, especially at low-intensity range $I\lambda^2 \leqslant 10^{18}$ W cm^{-2} μm^2, indicates that vacuum heating mechanism takes place. Moreover, we find in our simulation that the collision effect seems to suppress the vacuum heating process. It could be explained by the collision effect hindering the inside electrons from being pulled out of the target, since the collisional mean free path of electrons is estimated to be about 20 nm using the formula given by Beck *et al* [36], and this value is roughly one order of magnitude smaller than the penetration depth of the laser evanescent wave, which can be considered as a characteristic depth of laser–plasma interaction in vacuum heating. The case of $L = 1\lambda$ is given in figure 2(b). Obviously at 21.6°, which is close to the optimum incident angle for resonance absorption $\theta_m = \arcsin[0.68(\omega L/c)^{-1/3}]$ [37], the laser energy is absorbed much more strongly, demonstrating that resonance absorption occurs and contributes most of the absorption. With the collisional effect included, the damping rate of the excited ESW will be larger and the resonance absorption is expected to be enhanced, this is verified by comparing the black solid line and the dashed purple line in figure 2(b). The other non-collisional behavior of resonance absorption under different laser and target parameters has already been considered numerically by Ding *et al* [18].
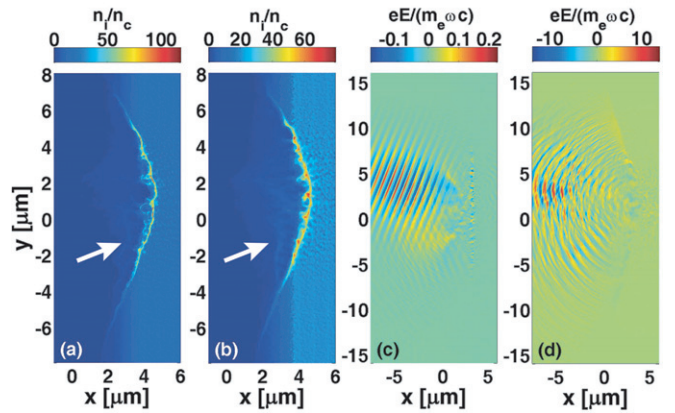

Figure 3. Snapshot of the ion density for the collisionless case (a) or collisional case (b) at the moment while the reflected part of the laser pulse just leaves the target surface at laser intensity $I\lambda^2 = 1.37 \times 10^{20}$ W cm^{-2} μm^2. Snapshots of the electric field of the reflected laser at intensity 1.37×10^{16} W cm^{-2} μm^2 (c) and 1.37×10^{20} W cm^{-2} μm^2 (d), for the preplasma density scale length $L = \lambda$ and laser incident direction shown by the arrows.

When the laser intensity increases to 10^{18} W cm^{-2} μm^2 and above, the electrons will be pushed toward the laser-incident direction by the very strong ponderomotive force, as shown later in section 3 in detail. This leads to a significant increase in absorption rate. An obvious increase in the absorption rate is seen for long density scale length L. In our simulation, an absorption rate as high as 90% is observed for $L = 4\lambda$ at $I\lambda^2 = 1.37 \times 10^{20}$ W cm^{-2} μm^2.

The increase in laser absorption with the density scale length is associated with the hole boring effect. As shown in figures 3(a) and (b), hole boring enables the laser pulse to propagate deeper into the target and interact with the plasma more adequately, leading to enhanced absorption [22, 26]. Figures 3(c) and (d) give the reflected laser field at intensities 1.37×10^{16} W cm^{-2} μm^2 and 1.37×10^{20} W cm^{-2} μm^2, respectively. We find the hole boring effect significantly distorts the reflected pulse. Our simulations also show that if the collision is included, the high-density layer formed by laser
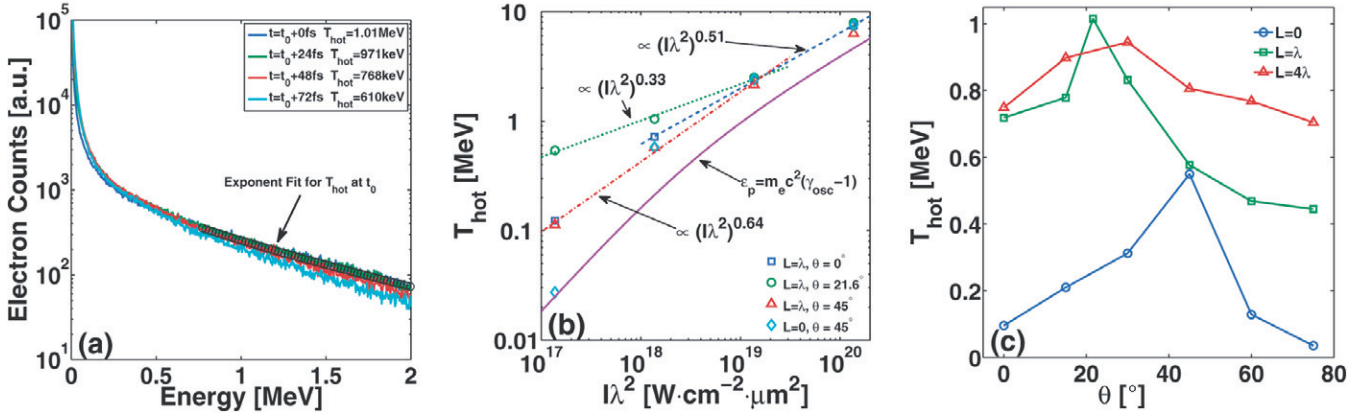
Figure 4. (*a*) Typical energy spectrum evolution after t_0, where t_0 represents the time when the reflected laser pulse just leaves the target surface completely. The laser is incident at 21.6° with intensity 1.37×10^{18} W cm^{-2} μm^2 and the preplasma density scale length is λ. (*b*) Hot electron temperatures versus incident laser intensity under different parameters. The dashed, dotted and dashed–dotted lines are power fittings of the corresponding data points. Note that at intensities 10^{19} and 10^{20} W cm^{-2} μm^2, the temperatures under different laser incident angles and preplasma conditions are almost identical. (*c*) Angular dependence of hot electron temperature at incident intensity 1.37×10^{18} W cm^{-2} μm^2.

pressure is widened and the peak density decreases drastically. This might be a potential explanation of the 1–2% increase in the absorption rate when collision effect is included. In addition, one may find from Davies' review paper [27] that absorption rates obtained from long pulse experiments are generally lower than those from the experiments (e.g. [26]) and simulations (e.g. figure 2) using short pulses, especially for ultrahigh intensities ($I\lambda^2 > 10^{19}$ W cm^{-2} μm^2). This could also be partially explained by the formation of high density layers at the target front, which may reduce considerably the absorption of the rear part of the laser pulse when it is relatively long. Parametric instabilities [38, 39] can also develop during the long pulse propagation and further decrease the absorption.

For small incident angles ($\leqslant 45°$), our simulation result shows a flat angular dependence at relativistic intensities, which is consistent with the analytical model derived by Gibbon *et al* [23]. However, at large incident angles, the absorption rates decrease significantly due to the weakening of the hole boring effect as well as smaller penetration depth when the preplasma exists. This decrease deviates from their model because they did not take the effect of ion motion and preplasma into consideration. It could be expected that the deviation will be smaller if heavier ion species and higher plasma densities are used.

3. Hot electron temperature scalings and angular distributions

The laser absorption leads to hot electron production directly, especially when the laser intensity is higher, over 10^{17} W cm^{-2}. Different laser intensities also lead to different hot electron temperature scalings. Figure 4(*a*) gives a typical time evolution of electron energy spectrum after t_0, where t_0 represents the time when the reflected laser pulse just leaves the target surface. Hot electron temperatures under different laser and target parameter sets at t_0 are summarized in figure 4(*b*). We found while the incident angle matches the optimized angle $\theta_m = \arcsin[0.68(\omega L/c)^{-1/3}]$, i.e. resonance
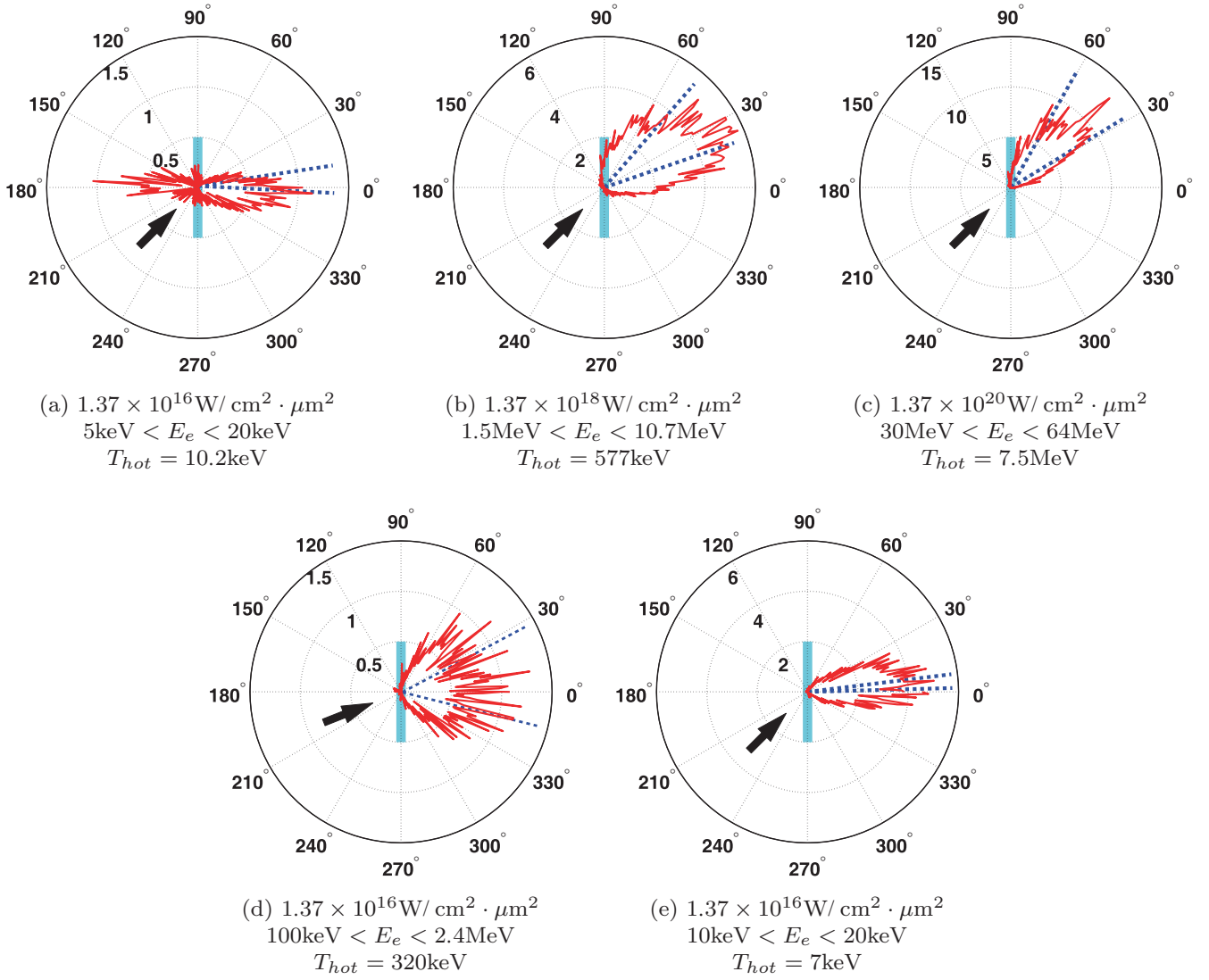
absorption dominates the absorption process at low incident laser intensities, the hot electron temperature satisfies

$$T_{\text{hot}} = \left(\frac{I\lambda^2}{10^{18} \text{ W cm}^{-2} \, \mu\text{m}^2} \right)^{1/3} \times 1.01 \, \text{MeV}, \qquad (2)$$

which agrees with the scale law by Beg *et al* [25, 40]. It is worth mentioning that other measurements in Beg's experiment which gave the 1/3 scaling law also suggested an important role of resonance absorption.

One notes that the coefficient 1.01 MeV obtained by our simulations in equation (2) is nearly 5 times larger than Beg's inference from their experiment. This could be attributed to the following three reasons. Firstly, the hot electron temperature given by equation (2) is found just after the laser interaction. As shown in figure 4(*a*), there is an obvious decrease in hot electron temperatures within less than 100 fs after t_0 due to collision with cold ions and other dissipative processes such as the hot electron transport through dense plasma [41]. For example, at 72 fs after the laser interaction, the hot electron temperature is already reduced to 610 keV. Secondly, usually a relatively higher background electron temperature is chosen in simulations. According to the theory given by Forslund *et al*, such a choice can lead to a higher hot electron temperature in the resonance absorption [42]. Lastly, the results we give here are obtained under the optimized resonance condition for the incident angle and the plasma scale length. However, this condition is usually not fulfilled in the experiment. If this condition is slightly deviated from, there will still be such a scaling with the laser intensity, but the constant number will become smaller. A more detailed discussion of this effect is addressed in the next paragraph.

In order to verify the last reason listed above, we have performed another group of simulations in which the incident angles and preplasma scale lengths are slightly mismatched. The simulation gives a much smaller coefficient 0.71 MeV at the time when the laser pulse just reflects from the target, for example. In the meanwhile, the power exponent of $I\lambda^2$ is also

Figure 5. Angle distributions of hot electrons at different intensities for a certain electron energy range. The laser incident angle is 45° and the preplasma scale length is λ for (*a*), (*b*), (*c*). (*d*) The condition when resonance absorption dominates the absorption with incident angle 21.6° and scale length $L = 1\lambda$. (*e*) Vacuum heating without preplasma and 45° incidence. The dashed lines in each plot denote the angular range estimated by equation (2).

slightly increased to 0.35. This increase can be interpreted as follows. Intuitively, one can expect that as the deviation from the optimized condition of resonance absorption becomes large, the temperature of hot electrons produced by resonance absorption will become low, in particular in the low laser-intensity range. On the other hand, along with the increase in incident laser intensity, the dominant absorption mechanism gradually converts to $j \times B$ heating and ponderomotive acceleration, so the hot electron temperature becomes less affected by the decrement of resonance absorption. Because of this interplay between different absorption mechanisms, one can infer that the power exponent of $I\lambda^2$ will get larger along with the deviation from the optimized condition of resonance absorption. For example, we find in our simulation that the hot electron temperature scaling changes to $\sim(I\lambda^2)^{0.64}$ under 45° incidence and 1λ preplasma density scale length, which is shown by the red triangles in figure 4(*b*). A recent experiment performed by Mordovanakis *et al* also obtained this power exponent under similar intensity range and incident angle [29].

A more detailed scan of the angular dependence of T_{hot} at $1.37 \times 10^{18} \text{ W cm}^{-2} \mu\text{m}^2$ is also addressed in figure 4(*c*), in which one can see the noticeable increase caused by the resonance absorption. When the resonance condition is not satisfied, T_{hot} generally increases with the incident angle at first and then decreases, indicating that there is an optimal incident angle for hot electron generation.

At normal incidence, there is almost no resonance absorption, ponderomotive force dominates the acceleration. T_{hot} becomes proportional to $(I\lambda^2)^{1/2}$ when the incidence reaches $10^{18} \text{ W cm}^{-2} \mu\text{m}^2$ [22]. The solid line in figure 4(*b*) shows an estimate of T_{hot} by ponderomotive potential, i.e. the energy of electrons oscillating in the transverse field of the incident light wave $\varepsilon_{\text{p}} = (\gamma_{\text{osc}} - 1)m_{\text{e}}c^2$, where $\gamma_{\text{osc}} = [1 + I\lambda^2/(1.37 \times 10^{18} \text{ W cm}^{-2} \mu\text{m}^2)]$. Being in accord with Wilks *et al* [22], T_{hot} given by our simulation is also a bit larger than ε_{p} with $T_{\text{hot}} \simeq 2\varepsilon_{\text{p}}$. Again, this value is larger than the values given by Sherlock [41]. This could also be attributed to the earlier time when the measure is carried out,

which excludes the subsequent loss in energy of electrons due to dissipative processes mentioned before (see the second paragraph of section 3). It is expected that a larger density scale length and a longer pulse duration can lead to similar scaling multiplied by higher numerical factors.

The cyan diamonds in figure 4(*b*) gives the results in the case when preplasma does not exist. At high incident intensities, the scaling of the hot electron temperatures is close to the results with preplasma. But as the intensity decreases, corresponding to the case of vacuum heating, the hot electron temperature becomes much smaller than the case with preplasma, leading to a much larger power exponent of $I\lambda^2$. It is roughly calculated to be $T_{hot} \propto (I\lambda^2)^{1.32}$ if we use the data points at 10^{17} and 10^{18} W cm^{-2} μm^2. This shows that preplasma is very important in low-intensity absorption processes. Schnüere *et al* gave the scaling $T_{hot} \propto (I\lambda^2)^{1-1.5}$ from their experiment using a relatively high contrast laser (up to 10^{10} at 0.5 ns before the main pulse) [30], which is consistent with our simulation results.

The emission direction of the hot electrons is also measured in our simulation. It is believed to provide a signature of the dominant absorption rate [26], and it is also very important to the potential applications of the interaction between ultrashort ultra-intense laser and plasma. As shown in figures 5(*a*), (*d*) and (*e*), at low intensities, hot electrons generated by collisional absorption, resonance absorption and vacuum heating together are all emitting around the target normal, unrelated to the laser incident angle. This shows that under these mechanisms, the emission directions are not completely determined by the mechanisms. It has been shown before that the emission angle β is a function of electron energy $(\gamma - 1)m_e c^2$, where γ denotes the Lorentz factor of the hot electrons, laser incident angle θ and experienced quasi-static electric and magnetic fields inside the target by [43, 44]

$$\sin\beta = \frac{\gamma - 1 - \delta\Phi}{(\gamma^2 - 1)^{1/2}} \sin\theta, \qquad (3)$$

where $\delta\Phi = |e|[\delta\varphi - \delta A_{0y}/\sin\theta]/(m_e c^2)$ is the normalized potential exchange, $\delta\varphi$ and δA_{0y} denote the scalar and vector potential changes experienced by the particles. Path integration on each electron is needed to obtain the exact $\delta\Phi$ value [44], but its maximum value can be estimated simply by $|\delta\Phi_{max}| \sim T_{hot}$, where T_{hot} represents the temperature of the hot electrons [43]. By seeking the maximum and minimum of the function $\beta(\gamma, \delta\Phi)$ given by equation (3) in the region $\gamma_{min} \leqslant \gamma \leqslant \gamma_{max}$ for $-T_{hot} \leqslant \delta\Phi \leqslant T_{hot}$, we can give an estimation of the electron emission angle range, as shown by the dashed lines in figure 5. Here γ_{min} and γ_{max} correspond to the lower cut-off energy given in the caption of each subfigure and the maximal electron energy found in the simulation, respectively. However, the angle ranges estimated by equation (3) are generally smaller than the simulation results. At low laser intensities, this underestimation is partially due to the collisions, which can scatter the hot electrons to wider angular distributions. At high laser intensities, multi-dimensional effects can play a significant role, such as the target surface deformation and laser hole boring as shown in figure 3.

4. Conclusions

In conclusion, we investigate the absorption mechanisms in a wide intensity range via PIC simulation with the Coulomb collision effect included. Our simulation results show that usually collisional absorption dominates the low-intensity absorption mechanisms, but it gets weaker as the laser intensity increases and can be negligible when the laser intensity is larger than 10^{16} W cm^{-2} μm^2. When the incident angle is close to the optimized angle $\theta_m = \arcsin[0.68(\omega L/c)^{-1/3}]$, resonance absorption becomes the main absorption mechanism at low intensities and contributes 0.4–0.5 in the absorption rate. When the preplasma density scale length is much less than the laser wavelength, vacuum heating can occur. The collisional effect is observed to enhance the resonance absorption but suppress the vacuum heating process. At high intensities $I\lambda^2 \geqslant 10^{18}$ W cm^{-2} μm^2, the ponderomotive force accelerating and $\boldsymbol{j} \times \boldsymbol{B}$ heating absolutely dominate the absorption process and can lead to up to 90% of laser energy absorbed if the preplasma is relatively large. The angular distribution of generated hot electrons shows a strong dependence on the laser intensities.

The temperature of hot electrons obtained from our simulation shows a power scaling law with incident laser intensity by $T_{hot} \propto (I\lambda^2)^\alpha$. The value of α is determined by the dominant absorption mechanism. When the incident angle and the preplasma density scale length satisfy the optimized condition of resonance absorption, α is found to be 1/3, which is in accordance with scaling by Beg *et al* and Forslund *et al*. The deviation of the optimized condition will lead to a larger α value. Under the condition of $\boldsymbol{j} \times \boldsymbol{B}$ heating and ponderomotive acceleration dominance, our simulation gives $\alpha = 1/2$. For the vacuum heating case, α can be larger than 1, showing a much stronger dependence between hot electron temperature and incident laser intensity.

References

[1] Key M H 2001 *Nature* **412** 775–6
[2] Kodama R *et al* 2002 *Nature* **418** 933–4
[3] Silva L O, Marti M, Davies J R, Fonseca R A, Ren C, Tsung F S and Mori W B 2004 *Phys. Rev. Lett.* **92** 015002
[4] Clark E L *et al* 2000 *Phys. Rev. Lett.* **84** 670–3
[5] Maksimchuk A, Gu S, Flippo K, Umstadter D and Bychenkov V Y 2000 *Phys. Rev. Lett.* **84** 4108–11
[6] Chen M, Sheng Z M, Dong Q L, He M Q, Li Y T, Bari M A and Zhang J 2007 *Phys. Plasmas* **14** 053102–9
[7] Remington B A, Arnett D, Paul R, Drake and Takabe H 1999 *Science* **284** 1488–93
[8] Kahaly S, Yadav S K, Wang W M, Sengupta S, Sheng Z M, Das A, Kaw P K and Kumar G R 2008 *Phys. Rev. Lett.* **101** 145001
[9] Mondal S *et al* 2012 *Proc. Natl Acad. Sci.* **109** 8011–5
[10] Dawson J and Oberman C 1962 *Phys. Fluids* **5** 517–24
[11] Langdon A B 1980 *Phys. Rev. Lett.* **44** 575–9
[12] Gibbon P 1994 *Phys. Rev. Lett.* **73** 664–7

[13] Kruer W L 2003 *The Physics of Laser Plasma Interactions* (Boulder, CO: Westview)

[14] Gibbon P 2005 *Short Pulse Laser Interactions with Matter: An Introduction* (Singapore: World Scientific)

[15] Mulser P and Bauer D 2010 *High Power Laser–Matter Interaction (STMP 238)* (Berlin: Springer)

[16] Ma J X, Sheng Z M and Xu Z Z 1991 *Phys. Fluids* B **3** 3524–7

[17] Xu H, Sheng Z M, Zhang J and Yu M Y 2006 *Phys. Plasmas* **13** 123301

[18] Ding W J, Sheng Z M, Zhang J and Yu M Y 2009 *Phys. Plasmas* **16** 042315–4

[19] Brunel F 1987 *Phys. Rev. Lett.* **59** 52–5

[20] Gibbon P and Bell A R 1992 *Phys. Rev. Lett.* **68** 1535–8

[21] Kruer W L and Estabrook K 1985 *Phys. Fluids* **28** 430–2

[22] Wilks S C, Kruer W L, Tabak M and Langdon A B 1992 *Phys. Rev. Lett.* **69** 1383–6

[23] Gibbon P, Andreev A A and Platonov K Y 2012 *Plasma Phys. Control. Fusion* **54** 045001

[24] Price D F, More R M, Walling R S, Guethlein G, Shepherd R L, Stewart R E and White W E 1995 *Phys. Rev. Lett.* **75** 252–5

[25] Beg F N, Bell A R, Dangor A E, Danson C N, Fews A P, Glinsky M E, Hammel B A, Lee P, Norreys P A and Tatarakis M 1997 *Phys. Plasmas* **4** 447–57

[26] Ping Y *et al* 2008 *Phys. Rev. Lett.* **100** 085004

[27] Davies J R 2009 *Plasma Phys. Control. Fusion* **51** 014006

[28] Malka G and Miquel J L 1996 *Phys. Rev. Lett.* **77** 75–8

[29] Mordovanakis A G, Masson-Laborde P E, Easter J, Popov K, Hou B, Mourou G, Rozmus W, Haines M G, Nees J and Krushelnick K 2010 *Appl. Phys. Lett.* **96** 071109–3

[30] Schnurer M, Kalashnikov M P, Nickles P V, Schlegel T, Sandner W, Demchenko N, Nolte R and Ambrosi P 1995 *Phys. Plasmas* **2** 3106–10

[31] Chen M, Sheng Z M, Zheng J, Ma Y Y and Zhang J 2008 *Chin. J. Comput. Phys.* **25** 43

[32] Wang W M, Sheng Z M, Norreys P A, Sherlock M, Trines R, Robinson A P L, Li Y T, Hao B and Zhang J 2010 *J. Phys.: Conf. Ser.* **244** 022070

[33] Sentoku Y and Kemp A J 2008 *J. Comput. Phys.* **227** 6846–61

[34] Landau L D and Lifshitz E M 1981 *Physical Kinetics* (Oxford: Pergamon)

[35] Yang T Y B, Kruer W L, More R M and Langdon A B 1995 *Phys. Plasmas* **2** 3146–54

[36] Beck A and Meyer-Vernet N 2008 *Am. J. Phys.* **76** 934–6

[37] Ahedo E and Sanmartin J R 1987 *Plasma Phys. Control. Fusion* **29** 419

[38] Klimo O, Tikhonchuk V T, Ribeyre X, Schurtz G, Riconda C, Weber S and Limpouch J 2011 *Phys. Plasmas* **18** 082709–12

[39] Klimo O, Weber S, Tikhonchuk V T and Limpouch J 2010 *Plasma Phys. Control. Fusion* **52** 055013

[40] Haines M G, Wei M S, Beg F N and Stephens R B 2009 *Phys. Rev. Lett.* **102** 045008

[41] Sherlock M 2009 *Phys. Plasmas* **16** 103101–6

[42] Forslund D W, Kindel J M and Lee K 1977 *Phys. Rev. Lett.* **39** 284–8

[43] Sheng Z M, Sentoku Y, Mima K, Zhang J, Yu W and Meyer-ter Vehn J 2000 *Phys. Rev. Lett.* **85** 5340–3

[44] Chen M, Sheng Z M and Zhang J 2006 *Phys. Plasmas* **13** 014504–4